Correspondence between long-range and short-range spin glasses

R. A. Baños,[1,2] L. A. Fernandez,[3,2] V. Martin-Mayor,[3,2] and A. P. Young[4]
[1]*Departamento de Física Teórica, Universidad de Zaragoza, 50009 Zaragoza, Spain*
[2]*Instituto de Biocomputación y Física de Sistemas Complejos (BIFI), Zaragoza, Spain*
[3]*Departamento de Física Teórica I, Universidad Complutense, 28040 Madrid, Spain*
[4]*Department of Physics, University of California, Santa Cruz, California 95064, USA*
(Received 30 July 2012; published 17 October 2012)

We compare the critical behavior of the short-range Ising spin glass with a spin glass with long-range interactions which fall off as a power σ of the distance. We show that there is a value of σ of the long-range model for which the critical behavior is very similar to that of the short-range model in four dimensions. We also study a value of σ for which we find the critical behavior to be compatible with that of the three-dimensional model, although we have much less precision than in the four-dimensional case.

DOI: 10.1103/PhysRevB.86.134416 PACS number(s): 75.50.Lk, 75.40.Mg, 05.50.+q

I. INTRODUCTION

In the theory of systems at their critical point it is instructive to consider a range of dimensions d, since above an upper critical dimension d_u the critical behavior becomes quite simple and corresponds to that of mean-field theory. Hence it is desirable to understand critical behavior up to, and just above, $d = d_u$. For the case of spin glasses,[1] where much of what we know has come from numerical simulations, this has been difficult because (i) the value of d_u is quite large ($d_u = 6$ as opposed to 4 for conventional systems like ferromagnets) and (ii) the slow dynamics, coming from the complicated "energy landscape," prevents equilibration of systems with more than of order 10^4 spins at and below the transition temperature T_c. Since the total number of spins V is related to the linear size L by $V = L^d$, for dimensions around d_u (=6) it is then not possible to study a *range* of values of L, which, however, is necessary to carry out a finite-size scaling[2,3] (FSS) analysis.

It has been proposed[4] to try to circumvent this problem by using, instead, a one-dimensional spin-glass model in which the interactions J_{ij} fall off as a power of the distance, roughly $J_{ij} \sim 1/|r_i - r_j|^\sigma$, since varying σ in this one-dimensional (1D) model seems to be analogous to varying d in a short-range models. In both cases there is a range where there is no transition (d is below a lower critical dimension d_l, and σ greater than a certain value σ_l), a range where there is a transition with non-mean-field exponents ($d_l < d < d_u$, $\sigma_l > \sigma > \sigma_u$ for a certain σ_u which turns out to be 2/3), and a transition with mean-field exponents ($d_u < d < \infty$, $\sigma_u > \sigma > 1/2$). The advantage of the 1D model is that one can study a large range of linear sizes for the whole range of σ. Consequently, there have been several subsequent studies[5–12] on these models.

The question that we tackle here is whether this connection between long-range models in one dimension and short-range models in a range of dimensions is just a vague analogy or whether the connection can be made precise in the following sense: for a given d is there a value of σ such that *all* the critical exponents of the short-range model correspond with those of the long-range model [in the sense of Eq. (5) below]? We will denote the value of σ in Eq. (5) as a *proxy* for the dimension d.

A relation between the long-range (LR) and short-range (SR) exponents has been proposed in Ref. 8. We reproduce their argument here in a more general formulation. Consider the singular part of the free-energy density. For a system in d dimensions it has the scaling form

$$f_{\rm sing} = \frac{1}{L^d}\,\widetilde{f}(L^{y_T}t, L^{y_H}h, L^{y_u}u), \tag{1}$$

where $\widetilde{f}$ is a scaling function, $t \equiv (T - T_c)/T_c$ is the reduced temperature, h is the magnetic field (for a spin glass it is actually the variance of a random field), u is the operator which gives the leading correction to scaling, y_T is the thermal exponent, y_H is the magnetic exponent, and y_u (<0) is the exponent for the leading correction to scaling. These exponents can be expressed in terms of more commonly used exponents,

$$y_T = \frac{1}{\nu}, \quad y_H = \frac{1}{2}(d + 2 - \eta), \quad y_u = -\omega, \tag{2}$$

where ν is the correlation-length exponent, η describes the power-law decay of correlations at the critical point, and $\omega > 0$.

We make a connection between the two models by equating the singular part of their free-energy densities. Let V be the total number of spins (so $V = L^d$ in the short-range model, while $V = L$ for the long-range model). We compare the two free-energy densities for systems with the same number of spins $V = L_{\rm SR}^d = L_{\rm LR}$:

$$\frac{1}{L_{\rm SR}^d}\,\widetilde{f}_{\rm SR}\left(L_{\rm SR}^{y_T^{\rm SR}}t, L_{\rm SR}^{y_H^{\rm SR}}h, L_{\rm SR}^{y_u^{\rm SR}}u\right) = \frac{1}{L_{\rm LR}}\,\widetilde{f}_{\rm LR}\left(L_{\rm LR}^{y_T^{\rm LR}}t, L_{\rm LR}^{y_H^{\rm LR}}h, L_{\rm LR}^{y_u^{\rm LR}}u\right). \tag{3}$$

In order to compare exponents we need to eliminate the different prefactors in front of the scaling functions by writing everything in terms of the total number of spins. Canceling a factor of $1/V$ on both sides gives

$$\widetilde{f}_{\rm SR}\left(V^{y_T^{\rm SR}/d}t, V^{y_H^{\rm SR}/d}h, V^{y_u^{\rm SR}/d}u\right) = \widetilde{f}_{\rm LR}\left(V^{y_T^{\rm LR}}t, V^{y_H^{\rm LR}}h, V^{y_u^{\rm LR}}u\right). \tag{4}$$

Hence, for each of the exponents, the correspondence between the LR and SR values is

$$y_{\rm LR}(\sigma) = \frac{y_{\rm SR}(d)}{d}. \tag{5}$$

 ©2012 American Physical Society

We note that in the mean-field regime, $6 < d < \infty$, $2/3 > \sigma > 1/2$, Eq. (5) holds consistently[8] for the thermal, magnetic, and correction exponents with

$$d = \frac{2}{2\sigma - 1} \quad \text{(mean-field regime)}, \tag{6}$$

since[13,14] $\eta_{\rm SR} = 0, \eta_{\rm LR} = 3 - 2\sigma$, $\nu_{\rm SR} = 1/2$, $\nu_{\rm LR} = 1/(2\sigma - 1), \omega_{\rm SR} = (d-6)/2$, and $\omega_{\rm LR} = 2 - 3\sigma$. Furthermore, the exponents also match to first order in $6 - d$ for the SR model and $\sigma - 2/3$ for the LR model.[15] Actually, Eq. (5) (at least as applied to the thermal exponent $\nu = 1/y_T$) can be derived for all d and σ from a superuniversality hypothesis.[16]

In this paper we will investigate whether, for $d = 3$ and 4, we can find a value of σ which satisfies Eq. (5) simultaneously for the thermal, magnetic, and correction-to-scaling exponents.

One advantage of long-range systems is that the exponent η is known exactly, as was first shown by Fisher *et al.*[17] for ferromagnets. The result for spin glasses is

$$2 - \eta_{\rm LR}(\sigma) = 2\sigma - 1, \tag{7}$$

so Eq. (5) for the magnetic exponent y_H $(=(d + 2 - \eta)/2)$ can be written[8]

$$2\sigma - 1 = \frac{2 - \eta_{\rm SR}(d)}{d}, \tag{8}$$

which immediately gives us a value of σ that acts as a proxy for d provided we know $\eta_{\rm SR}(d)$. For $d = 3$, the values of $\eta_{\rm SR}$ as well as of other exponents have been determined accurately by Hasenbusch *et al.*,[18] and we use their values here. In particular, they find $\eta_{\rm SR}(3) = -0.375(10)$, which, according to Eq. (8), corresponds to a proxy value $\sigma = 0.896$. We shall therefore perform simulations for this value of σ to see if the other exponents, y_T and y_u, also match those of the $d = 3$ results[18] according to Eq. (5).

However, for $d = 4$, the values of $\eta_{\rm SR}$ and the other exponents are not known with great precision, so we carry out a careful study of this model here to determine them more accurately. We find $\eta_{\rm SR}(4) = -0.320(13)$ for which the proxy value of σ, according to Eq. (8), is $\sigma = 0.790$. We therefore also study this value of σ to see if the other exponents match those of the $d = 4$ simulations according to Eq. (5).

It is also convenient to note that Eq. (5) for the thermal exponent y_T $(=1/\nu)$ can be written

$$\nu_{\rm LR}(\sigma) = d\, \nu_{\rm SR}(d), \tag{9}$$

and, since $y_u = -\omega$, the connection between the correction-to-scaling exponents is

$$\omega_{\rm LR}(\sigma) = \frac{\omega_{\rm SR}(d)}{d}. \tag{10}$$

To summarize, the main goal of this paper is to see if there is a single value of σ which simultaneously satisfies Eqs. (8)–(10) for $d = 3$ and (with a different value of σ) for $d = 4$.

The plan of this paper is as follows. In Sec. II we describe the model and the observables we calculate. Section III discusses the finite-size-scaling analysis, while Sec. IV describes the details of the simulations. The results and analysis are presented in Sec. V, and our conclusions are summarized in Sec. VI.

II. MODEL AND OBSERVABLES

We consider the Edwards-Anderson spin-glass model with Hamiltonian

$$\mathcal{H} = -\sum_{\langle i,j \rangle} J_{ij} S_i S_j, \tag{11}$$

where the Ising spins S_i take values ± 1 and the quenched interactions J_{ij} are independent random variables, the form of which will be different for the different models that we study.

The first model is a nearest-neighbor spin glass in four dimensions in which the J_{ij} take values ± 1 with equal probability if i and j are nearest neighbors, and are 0 otherwise, i.e., the probability distribution is

$$P(J_{ij}) = \begin{cases} \frac{1}{2}[\delta(J_{ij} - 1) + \delta(J_{ij} + 1)] & (i,j \text{ neighbors}), \\ \delta(J_{ij}) & (\text{otherwise}). \end{cases} \tag{12}$$

The advantage of the ± 1 interactions is that we are able to use multispin coding,[19] in which the interactions and the spins are represented by a single bit rather than a whole word. In fact, our C code uses 128-bit words, using the streaming SIMD extensions, so we simulate 128 samples in parallel. In order to gain the full speedup, we use the *same* random numbers for each of the 128 samples in a "batch." Hence, while the results for each sample are unbiased, there may be correlations between samples in the same batch. Consequently, when we estimate error bars we first average over the samples in a batch and use this average as a single data point in the analysis. Data from different batches are uncorrelated.

The spins are on a four-dimensional hypercubic lattice of linear size L with periodic boundary conditions. The total number of spins is $V = L^4$.

The description of the interactions we take for the 1D models is a bit more complicated. The interactions must fall off with distance such that

$$\left[J_{ij}^2\right]_{\rm av} \propto \frac{1}{r_{ij}^{2\sigma}}, \tag{13}$$

where $r_{ij} = |r_i - r_j|$ [the $i = 0, 1, \ldots, L-1$ sites in the graph are placed in a circle of radius $L/(2\pi)$, and the site i is at angle $i 2\pi/L$]. On the other hand $[\cdots]_{\rm av}$ denotes an average over the interactions. The simplest way to do this is to have every spin interact with every other spin with an interaction strength which has zero mean and standard deviation proportional to $1/r_{ij}^{\sigma}$. However, this is inefficient to simulate for large sizes, because the CPU time per sweep is of order L^2, rather than Lz in short-range systems with coordination number z.[20] Fortunately, it was realized by Leuzzi *et al.*[10] that one can have the CPU time scale also as Lz for the long-range model if one dilutes it. In their version, most interactions are zero and those that are nonzero have a strength of unity (i.e., the strength does not decrease with distance). Rather it is the *probability* of the interaction being nonzero which deceases with distance. In the specific construction of Leuzzi *et al.*[10] there are a total of $Lz/2$ nonzero interactions with an *average* degree (i.e., coordination number) of z and the probability of a nonzero interaction given by

$$p_{ij} = 1 - \exp\left(-A/r_{ij}^{2\sigma}\right) \left(\simeq A/r_{ij}^{2\sigma} \text{ at large } r_{ij}\right), \tag{14}$$

where A is chosen so that the mean degree is equal to some specified value z.

In the Leuzzi *et al*. model, the degree is not the same for all sites but has a Poisson distribution with mean z. Since we wish to implement multispin coding, and since the computer code for this depends strongly on the degree (and gets complicated for large degree), we study, instead, a model with *fixed* degree.

Before discussing how we generate these bonds, we should discuss to what extent physical properties will be modified. In a recent work,[24] the critical properties of the fully interacting model were compared with those of the diluted model by Leuzzi *et al*. The computation was carried out in the limit of an infinite number of spin components. The main outcome of this analysis was that the critical exponents are the same (as suggested by universality), irrespective of the connectivity. There were some major differences only for $\sigma \geqslant 1$, that is, in the σ regime where no spin-glass transition arises. Here, we shall not consider such a large σ. On the other hand, the diluted model has been investigated in the nonextensive regime (i.e., $\sigma \leqslant 1/2$) for Ising spin glasses.[25] Not only universal quantities, but also the transition temperatures, turned out to be identical to those of the (infinite-range) Viana-Bray model.[26] Finally, one might question as well the effects of fixing the connectivity rather than letting it fluctuate. This problem was recently investigated for Ising spin glasses in the hypercube.[27] Fixing the connectivity does change the critical temperature. However, universal quantities such as the critical exponents are not modified by this choice. Furthermore, scaling corrections were found to be dramatically smaller for the fixed-connectivity model.

We are not aware of any simple algorithm to generate bonds of arbitrary length such that each site has a specified number of bonds (z here) and the probability of a bond between i and j varies with distance r_{ij} in some specified way ($\propto 1/r_{ij}^{2\sigma}$ here). We therefore construct the Hamiltonian for which we will simulate the spins by first performing a Monte Carlo simulation *of the bonds*. A similar (but simpler) problem was resolved in this way in Ref. 27. We take the "Hamiltonian" of the bonds to be given by

$$e^{-\mathcal{H}_{\rm bond}} = e^{-\sum_{\langle i,j\rangle} \epsilon_{ij} \ln r_{ij}^{2\sigma}} \prod_k \delta\left(\sum_l \epsilon_{kl} - z\right), \qquad (15)$$

where $\epsilon_{ij} = 0$ or 1, in which 1 represents a bond present between sites i and j, and 0 represents no bond. Graphically, we regard each site i as having z "legs" associated with it, and we initially pair up the legs in a random way, representing each connected pair graphically as an "edge" and giving the value $\epsilon_{ij} = 1$ to all edges while all other pairs (i,j) have $\epsilon_{ij} = 0$. We then run a Monte Carlo simulation in which the nonzero ϵ_{ij} are swapped according to a Metropolis probability for the Hamiltonian in Eq. (15). To maintain exactly z nonzero ϵ's for each site the basic move involves reconnecting *two* bonds as shown in the sketch in Fig. 1.

Specifically, we first choose site 1 in Fig. 1, with uniform probability among the L possible choices. Next, site 3 is chosen with probability proportional to $1/r^{2\sigma}$ (r is the distance between sites 1 and 3). Finally, site 2 (site 4) is chosen with uniform probability among the z "neighbors" of site 1 (site 3). Before the move is attempted, we need to check that the

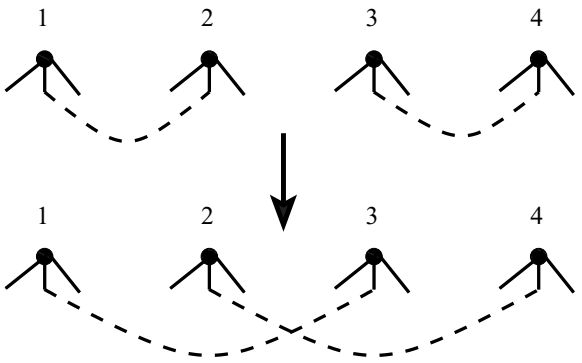

FIG. 1. Each site has a fixed number of "legs" (here we show three) and these legs are paired up by "edges." In the top row, one edge connects sites 1 and 2, and another edge connects sites 3 and 4. A basic Monte Carlo move for the bond-generation simulation consists of reconnecting two edges, as shown in the bottom row. (Other edges are present but not shown.)

sites 1, 2, 3, and 4 verify two consistency conditions. First, the four sites should be all different. Second, we require that neither sites 1 and 4, nor 2 and 3, are paired. If the consistency conditions are met, the basic move can be attempted and then be accepted or rejected with Metropolis probability. One *sweep* corresponds to Lz selection of sites of type 1 in Fig. 1.

After a suitable equilibration time,[28] we freeze the ϵ_{ij}, and the resulting set of nonzero ϵ_{ij} defines a "graph." Each of the 128 samples in a single batch of the multispin coding algorithm has the *same* graph. On the edges of the graph we put interactions with values ± 1 with equal probability chosen *independently* for each edge *in each sample* in a batch. The result is that the probability distribution *for a single bond* is given by

$$P(J_{ij}) = (1 - p_{ij})\delta(J_{ij}) + p_{ij}\tfrac{1}{2}[\delta(J_{ij} - 1) + \delta(J_{ij} + 1)], \qquad (16)$$

in which p_{ij} is given approximately by Eq. (14) for an appropriate choice of A corresponding to the specified value of z. However, the bonds are no longer statistically independent; rather there are correlations which ensure that each site has exactly z nonzero bonds. For both $\sigma = 0.896$ and 0.790 we take $z = 6$ neighbors.

We now describe the quantities that we calculate in the simulations. The spin-glass order parameter is

$$q = \frac{1}{V}\sum_{i=1}^{V} S_i^{(1)} S_i^{(2)}, \qquad (17)$$

where "(1)" and "(2)" are two identical copies of the system with the same interactions. Its Fourier transform to wave vector $\boldsymbol{k}$ is denote by $q(\boldsymbol{k})$. We will calculate the spin-glass susceptibility

$$\chi_{\rm SG} = V[\langle q^2\rangle]_{\rm av}, \qquad (18)$$

and also its wave-vector-dependent generalization,

$$\chi_{\rm SG}(\boldsymbol{k}) = V[\langle |q(\boldsymbol{k})|^2\rangle]_{\rm av}. \qquad (19)$$

From this we can extract the correlation length,[3,29–31]

$$\xi_L = \frac{1}{2\sin(\pi/L)}\sqrt{\frac{\chi(0)}{\chi(\boldsymbol{k}_1)} - 1}, \tag{20}$$

where $\boldsymbol{k}_1$ is the smallest nonzero wave vector, $\boldsymbol{k}_1 = (2\pi/L)(1,0,0,0)$ for the 4D model and $k_1 = 2\pi/L$ for the long-range models in 1D. Other quantities that we calculate, important because they are dimensionless like ξ_L/L, are the moment ratios

$$U_4 = \frac{[\langle q^4\rangle]_{\rm av}}{[\langle q^2\rangle]^2_{\rm av}}, \tag{21}$$

$$U_{22} = \frac{[\langle q^2\rangle^2]_{\rm av} - [\langle q^2\rangle]^2_{\rm av}}{[\langle q^2\rangle]^2_{\rm av}}, \tag{22}$$

and the susceptibility ratio

$$R_{12} = \frac{\chi_{\rm SG}(\boldsymbol{k}_1)}{\chi_{\rm SG}(\boldsymbol{k}_2)}, \tag{23}$$

where $\boldsymbol{k}_2$ is the second smallest nonzero wave vector, $\boldsymbol{k}_2 = (2\pi/L)(1,1,0,0)$ for the 4D model and $k_2 = 4\pi/L$ for the long-range models. We will also determine derivatives with respect to β of several of these quantities, using the result

$$\left\langle \frac{\partial O}{\partial \beta} \right\rangle = \langle O\mathcal{H}\rangle - \langle O\rangle\langle \mathcal{H}\rangle. \tag{24}$$

III. FINITE-SIZE-SCALING ANALYSIS

Using data from finite sizes, we have to extract the transition temperature $T_{\rm c}$, the correction-to-scaling exponent ω (since corrections to scaling are significant), the correlation-length exponent ν, and (for the short-range model for which the value is not known exactly) the exponent η. In this section we show how to include the *leading* correction to FSS. There are several sources of subleading corrections which will not be included in the formulas in this section, although we will try to include them empirically in some of the fits to the data, as discussed later in the section.

It is desirable to compute the various quantities one at a time so the value of the exponents depend on each other to the least extent possible. We therefore adopt the following procedure. We start with the finite-size-scaling form of a *dimensionless* quantity, since these quantities are simpler to analyze than those with dimensions and so they form the core of our analysis.

Dimensionless quantities are scale invariant, which means that at $T_{\rm c}$ they remain finite (neither zero nor infinite) in the limit of large L. However, dimensionless quantities are not only scale invariant, they are also *universal* (i.e., they remain constant under renormalization-group transformations). Examples of dimensionless quantities are ξ_L/L, U_4, U_{22}, and R_{12}. The distinction among scale-invariant and dimensionless quantities has been stressed in Ref. 18. Here we will discuss dimensionless quantities, but will comment on quantities which are scale invariant but not dimensionless in the last paragraph of this section.

A dimensionless quantity $f(L,t)$ has the FSS scaling form[31–33]

$$f(L,t) = \widetilde{F}_0(L^{1/\nu}t) + L^{-\omega}\widetilde{F}_1(L^{1/\nu}t), \tag{25}$$

where ω is the correction-to-scaling exponent, and

$$t = \frac{T - T_{\rm c}}{T_{\rm c}}. \tag{26}$$

We are interested in the behavior at large L and small t, and including just the leading corrections in $1/L$ and t gives

$$f(L,t) \simeq \widetilde{F}_0(0) + L^{1/\nu}t\,\widetilde{F}_0'(0) + L^{-\omega}\widetilde{F}_1(0). \tag{27}$$

It will be useful to determine the values of t_L^* where the quantity f takes the same value for sizes L and sL, where s is a scale factor which we shall take to be 2 here. We have

$$\begin{aligned}&\widetilde{F}_0(0) + L^{1/\nu}t_L^*\,\widetilde{F}_0'(0) + L^{-\omega}\widetilde{F}_1(0)\\ &\quad= \widetilde{F}_0(0) + (sL)^{1/\nu}t_L^*\,\widetilde{F}_0'(0) + (sL)^{-\omega}\widetilde{F}_1(0),\end{aligned} \tag{28}$$

which gives

$$\frac{T_L^* - T_{\rm c}}{T_{\rm c}} \equiv t_L^* = A_s^f L^{-\omega-1/\nu}, \tag{29}$$

or equivalently, to leading order,

$$\frac{\beta_{\rm c} - \beta_L^*}{\beta_{\rm c}} = A_s^f L^{-\omega-1/\nu}, \tag{30}$$

where the nonuniversal amplitude is given by

$$A_s^f = \frac{(1 - s^{-\omega})\,F_1(0)}{(s^{1/\nu} - 1)\,F_0'(0)}. \tag{31}$$

One can use Eq. (30) to locate $\beta_{\rm c}$. As we shall see, the exponents ω and $1/\nu$ are determined separately, and we use those values when fitting the data to Eq. (30).

We shall determine the critical exponents using the quotient method,[33] which is a more modern form of Nightingale's phenomenological renormalization.[34] First we determine the correction exponent ω by applying the quotient method to dimensionless quantities. Consider a second dimensionless quantity $g(L,t)$ which varies near $T_{\rm c}$ in the same way as f in Eq. (27), i.e.,

$$g(L,t) \simeq \widetilde{G}_0(0) + L^{1/\nu}t\,\widetilde{G}_0'(0) + L^{-\omega}\widetilde{G}_1(0). \tag{32}$$

Now compute $g(L,t)$ at t_L^*, given by Eq. (30), the temperature where results for L and sL intersect for some *different* dimensionless quantity f. We have

$$g(L,t_L^*) \simeq \widetilde{G}_0(0) + A_s^{g,f}L^{-\omega}, \tag{33}$$

where $A_s^{g,f} = A_s^f\,\widetilde{G}_0'(0) + \widetilde{G}_1(0)$. While this could be used directly to determine ω it is more convenient to take the ratio (quotient) of this result with the corresponding result for size sL, i.e.,

$$Q(g) \equiv \frac{g(sL,t_L^*)}{g(L,t_L^*)} = 1 + B_s^{g,f}L^{-\omega}, \tag{34}$$

where the amplitude $B_s^{g,f}$ is nonuniversal (because of the definition, it is zero if the quantities f and g are the same). Equation (34) is the most convenient expression from which to determine ω since it just involves the one unknown exponent

ω, and one amplitude B. These quantities can be determined by a straight-line fit to a log-log plot of $Q(g) - 1$ against L.

To determine the other exponents ν and η we need to consider the FSS form of quantities which *have* dimensions. Consider some quantity O which diverges in the bulk as t^{-x_O}. Including the leading correction it has the FSS form

$$O(L,t) = L^{y_O}[\widetilde{O}_0(L^{1/\nu}t) + L^{-\omega}\widetilde{O}_1(L^{1/\nu}t)], \qquad (35)$$

where $y_O = x_O/\nu$. Repeating the above arguments, and determining O for sizes L and sL at the intersection temperature t_L^* for the dimensionless quantity f for sizes L and sL, the quotient can be written as

$$Q(O) \equiv \frac{O(sL,t_L^*)}{O(L,t_L^*)} = s^{y_O} + B_s^{O,f}L^{-\omega}. \qquad (36)$$

Using the value of ω determined from Eq. (34) the exponent y_O is determined from Eq. (36) by a straight-line fit to a plot of $Q(O)$ against $1/L^\omega$.

To determine η we can use Eq. (36) for the spin-glass susceptibility $\chi_{\rm SG}$, since $y_O = 2 - \eta$ because the susceptibility exponent γ $(\equiv x_{\chi_{\rm SG}}) = (2-\eta)\nu$. To determine ν we note that ξ_L/L is dimensionless and so has the same FSS form as in Eq. (25). Differentiating, for instance, ξ_L with respect to β brings down a factor of $L^{1/\nu}$ and so $y_O = 1 + 1/\nu$ in this case ($y_O = 1/\nu$ if we take the *logarithmic* derivative). Hence we determine $1 + 1/\nu$ from Eq. (36) with O given by the β derivative of ξ_L.

To conclude, to carry out the FSS analysis we do the following steps:

(1) Determine ω from Eq. (34) for one or more dimensionless quantities f.

(2) Using the value of ω so determined, obtain $1 + 1/\nu$ (and $2 - \eta$ where necessary) from Eq. (36) with $O = \chi_{\rm SG}$ and $O = \partial\xi_L/\partial\beta$, respectively.

(3) Using the value of ω from stage III and $1/\nu$ from stage III, determine $\beta_{\rm c}$ from Eq. (30).

The error bars for $1 + 1/\nu$ and $2 - \eta$ from stage III will have a systematic component, coming from the uncertainty in the value of ω from stage III, as well as a component from statistical errors in the data being fitted. Similarly, the error bar in $\beta_{\rm c}$ from stage III will have a systematic component due to uncertainty in the value of $\omega + 1/\nu$.

Each of these three stages requires only a straight-line fit. However, in practice things are a little more tricky. We would like to use data for as many sizes as possible, but in practice the smaller sizes are affected by subleading corrections to scaling so we can use data only for the larger sizes. It is therefore necessary to include only a range of sizes for which the quality of the fit is satisfactory.

In some cases we try to incorporate a subleading correction to scaling to increase the range of sizes that can be used. These are of different types, one of which involves higher powers of the leading correction, and this is the only one we will include here in order to avoid introducing too many additional parameters. In other words, when we include subleading corrections we will do a *parabolic*, rather than linear, fit to the data as a function of $1/L^\omega$.

In order to increase the number of data points relative to the number of fit parameters, we will often do a combined fit to several data sets. For example, when estimating ω we will determine β_L^* from one dimensionless quantity f, and then determine two (or more) other dimensionless quantities at these temperatures. These data sets will be simultaneously fitted to Eq. (34) with the same value for ω (since this is universal) but different amplitudes B (since these are nonuniversal). Hence, by combining two data sets, we double the amount of data without doubling the number of fit parameters. It should be mentioned that, for a given size, the data for the different data sets are correlated, and the best estimates of fitting parameters are obtained by including these correlations.[33,35,36] In other words, if a data point is (x_i, y_i), and the fitting function is $u(x)$, which depends on certain fitting parameters, we determine those parameters by minimizing

$$\chi^2 = \sum_{i,j}[y_i - u(x_i)](C^{-1})_{ij}[y_j - u(x_j)], \qquad (37)$$

where

$$C_{ij} = \langle y_i y_j\rangle - \langle y_i\rangle\langle y_j\rangle \qquad (38)$$

is the covariance matrix. If there are substantial correlations in many elements, the covariance matrix can become singular, but we have checked that this is not the case for the quantities we study.

We end this section by discussing the FSS of a scale-invariant (but dimensionful) quantity, which turns out to be useful in our study of the LR model. Take Eq. (35) and imagine that we know exactly the exponent y_O. Then, $O(L,t)/L^{y_O}$ is scale invariant, since it remains finite at $t = 0$ even in the limit of large L. This is precisely the situation in the LR model, if we take for O the spin-glass (SG) susceptibility, because, as explained in the Introduction, the anomalous dimension is a known function of σ for those models. Nonetheless, Eq. (25) needs to be modified when applied to $\chi_{\rm SG}/L^{2\sigma-1}$, because the magnetic scaling field $u(h,t)$ is not exactly h, as assumed in Eq. (1) (see, e.g., Refs. 3 and 18). Rather, there is a nonlinear dependency on the thermodynamic control parameters t and h: $u_h(h,t) = h\tilde{u}_h(t) + \mathcal{O}(h^3)$, where $\tilde{u}_h(t) = 1 + c_1 t + c_2 t^2 + \cdots$. Hence, the analog of Eq. (25) reads

$$\frac{\chi_{\rm SG}(L,t)}{L^{2\sigma-1}} = \tilde{u}_h^2(t)[\widetilde{O}_0(L^{1/\nu}t) + L^{-\omega}\widetilde{O}_1(L^{1/\nu}t)]. \qquad (39)$$

We note that the multiplicative renormalization $\tilde{u}_h^2(t)$ cancels out when looking for crossing points, namely,

$$\frac{\chi_{\rm SG}(L,t_L^*)}{L^{2\sigma-1}} = \frac{\chi_{\rm SG}(sL,t_L^*)}{(sL)^{2\sigma-1}}, \qquad (40)$$

so t_L^* scales as in Eq. (30). Unfortunately, the multiplicative renormalization can no longer be ignored when we compute $1/\nu$ from $\partial_\beta\chi_{\rm SG}/L^{2\sigma-1}$. Indeed, differentiating Eq. (39) with respect to β and neglecting terms of order $1/L^{\omega+1/\nu}$, we find

$$\frac{\partial_\beta\chi_{\rm SG}(L,t)}{L^{2\sigma-1}} = L^{1/\nu}\big[\tilde{u}_h^2(t)\widetilde{O}_0'(L^{1/\nu}t) + L^{-\omega}\tilde{u}_h^2(t)\,\widetilde{O}_1'(L^{1/\nu}t) + L^{-1/\nu}2\tilde{u}_h(t)\tilde{u}_h'(t)\,\widetilde{O}_0(L^{1/\nu}t)\big], \qquad (41)$$

rather than Eq. (35). Both $\tilde{u}_h$ and $\tilde{u}_h'$ behave as L-independent constants (up to corrections of order $1/L^{\omega+1/\nu}$) when evaluated

at the crossing point t_L^* given in Eq. (30). Hence, the quotient of the β derivative of $\ln \chi_{SG}$ is given by

$$Q(\partial_\beta \ln \chi_{SG}) = s^{1/\nu} + B_1 L^{-\omega} + B_2 L^{-1/\nu}, \qquad (42)$$

instead of Eq. (36), showing that there are corrections of order $L^{-1/\nu}$ as well as $L^{-\omega}$. For some values of σ, and also the 3D SR model,[18] one finds $1/\nu < \omega$ so the $L^{-1/\nu}$ correction dominates.

IV. SIMULATION DETAILS

For each size and temperature we simulate four copies of the spins with the same interactions. By simulating four copies we can calculate, without bias, quantities which involve a product of up to four thermal averages, such as the spin-glass susceptibility, Eq. (18), the U_4 moment ratio, (21), and derivatives of these quantities with respect to β calculated from Eq. (24).

The simulations use parallel tempering[37] (PT) to speed up equilibration. For the same set of interactions we study N_β values of β between β_{max} and β_{min}. To obtain good statistics we simulate a large number N_{samp} of samples, where N_{samp} is a multiple of 128 because 128 samples are simulated in parallel by multispin coding. For the long-range models there are $N_{samp}/128$ different graphs, but each sample for the same graph has different interactions. We run for N_{sweep} single-spin flip (Metropolis) sweeps performing a parallel tempering sweep every ten Metropolis sweeps. The parameters used for the different models are shown in Tables I–III.

To check that the simulations were run for long enough to ensure equilibration we adopted the following procedure. We divide the measurements into bins whose size varies logarithmically; the first averages over the last half of the sweeps, i.e., between sweeps N_{sweep} and $N_{sweep}/2$, the second averages between sweeps $N_{sweep}/2$ and $N_{sweep}/4$, the third between sweeps $N_{sweep}/4$ and $N_{sweep}/8$, etc. We require that the difference between the results in the first two bins is zero within the error bars, where we get the error bar for the difference by forming the difference between the results for the two bins separately for each sample before averaging over samples. In most cases, to be on the safe side, we actually require that the differences between the first *three* bins are all zero within errors.

This procedure is illustrated in Fig. 2 which shows data for the long-range model with $L = 4096$ and $\sigma = 0.896$ at $\beta = 1.2$, the largest β value that we studied. The vertical axis is the difference in ξ_L/L between the bin containing measurements in sweeps $N_{MCS}/2$ to N_{MCS} (MCS indicates Monte Carlo Sweeps) and the bin for sweeps in the interval $N_{MCS}/4$ to $N_{MCS}/2$, for different values of N_{MCS} up to $N_{sweep} = 8.192 \times 10^7$, the value in Table III. Since the two points for the largest number of sweeps are zero within errors, it follows that the first three bins all agree.

TABLE I. Parameters of the simulations of the 4D model: N_β is the number of temperatures with β_{max} the largest and β_{min} the smallest. The number of Metropolis sweeps is given by N_{sweep}, and the number of samples is N_{samp}. The (inverse) temperature grid was optimized for $L = 16$, and kept fixed for smaller L. As a rule, the β spacing was 0.05. However, in order to reduce interpolation errors, the four largest β's are spaced by 0.025.

L	N_{sweep}	N_β	β_{max}	β_{min}	N_{samp}
4	2.56×10^5	23	0.5025	0.4	2^{20}
5	2.56×10^5	23	0.5025	0.4	2^{20}
6	2.56×10^5	23	0.5025	0.4	2^{20}
8	2.56×10^5	23	0.5025	0.4	2^{20}
10	2.56×10^5	23	0.5025	0.4	2^{20}
12	2.56×10^5	23	0.5025	0.4	2^{20}
16	5.12×10^5	23	0.5025	0.4	2^{20}

TABLE II. Parameters of the simulations of the 1D model with $\sigma = 0.790$. See Table I for an explanation of the symbols. The (inverse) temperature grid was optimized for $V = 32\,768$, and kept fixed for the smaller systems. We choose the grid in such a way that the acceptance in the parallel tempering move was roughly 20%. Empirically, this was achieved by decreasing the β spacing as a geometric progression with common ratio 0.98 (the largest spacing was for the highest β).

L	N_{sweep}	N_β	β_{max}	β_{min}	N_{samp}
512	10^6	16	0.671	0.538	64000
1024	10^6	16	0.671	0.538	64000
2048	10^6	16	0.671	0.538	64000
4096	1.28×10^6	16	0.671	0.538	64000
8192	1.28×10^6	16	0.671	0.538	64000
16384	2×10^6	16	0.671	0.538	64000
32768	2×10^6	16	0.671	0.538	64000

V. RESULTS

A. Four-dimensional short-range model

Figures 3 and 4 show results for ξ_L/L defined in Eq. (20) and Fig. 5 shows results for the dimensionless ratio of moments U_4 defined in Eq. (21). The resulting inverse temperatures β_L^* where data for sizes L and $2L$ intersect, i.e., where their quotient Q is unity, is shown in Table IV. Results are given for both ξ_L/L and U_4.

To compute the correction-to-scaling exponent ω we determine the quotient of ξ_L/L at the U_4 crossing and vice versa. These quotients are shown in Table V and plotted in Fig. 6. Fitting the largest two pairs of sizes for each quantity

TABLE III. Parameters of the simulations of the 1D model with $\sigma = 0.896$. See Table I for an explanation of the symbols. The β spacing was uniform up to $L = 1024$. For $L = 2048$ the β spacing ranges from 0.03 to 0.05, while it goes from 0.03 to 0.04 for $L = 4096$ and from 0.02 to 0.03 for $L = 8192$.

L	N_{sweep}	N_β	β_{max}	β_{min}	N_{samp}
512	1.28×10^6	16	1.5	0.6	12800
1024	2.56×10^6	13	1.2	0.6	12800
2048	1.024×10^7	14	1.2	0.65	12800
4096	8.192×10^7	16	1.2	0.65	12800
8192	8.192×10^7	16	1.1	0.71	12800

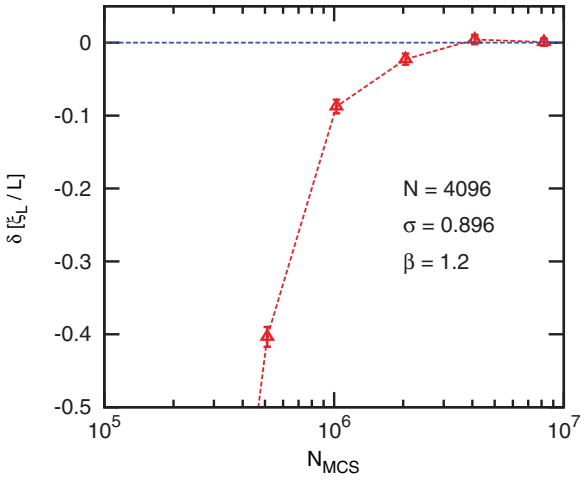

FIG. 2. (Color online) The difference in the values of ξ_L/L between measurements obtained in the range of sweeps $N_{\rm MCS}/2$ to $N_{\rm MCS}$ and measurements in the range $N_{\rm MCS}/4$ to $N_{\rm MCS}/2$, for values of $N_{\rm MCS}$ increasing by factors of 2 up to $N_{\rm sweep} = 8.192 \times 10^7$. The data are for the long-range model with $\sigma = 0.896$ at $\beta = 1.2$, the lowest temperature studied.

to Eq. (34) for $s = 2$ with the same exponent ω gives

$$\omega_{\rm SR}(4) = 1.04(10), \quad \chi^2/\mathcal{N}_{\rm DOF} = 0.99/1, \tag{43}$$

where $N_{\rm DOF}$ is the number of degrees of freedom, and χ^2 is defined in Eq. (37). It should be mentioned that the lines in Fig. 6 are not separate fits to each set of data but are combined fits including the whole covariance matrix.

We have also tried fits including subleading corrections to scaling. For instance, considering, in addition, the quotient of R_{12}, defined in Eq. (23), at the crossings of ξ_L/L and U_4, and fitting the three largest sizes to $1 + B_1 L^{-\omega} + B_2 L^{-2\omega}$ gives a satisfactory fit with $\omega = 1.29(26)$, $\chi^2/\mathcal{N}_{\rm DOF} = 2.26/5$. However, we prefer the result $\omega = 1.04(10)$ since it has been obtained using larger lattices ($L \geqslant 6$).

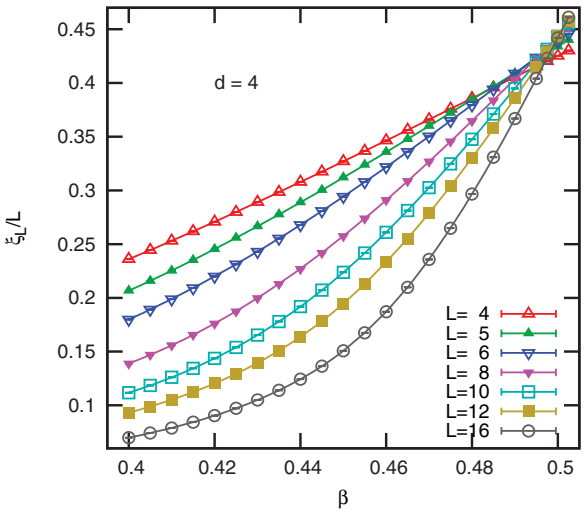

FIG. 3. (Color online) A global view of the data for the correlation length divided by L for the 4D model.

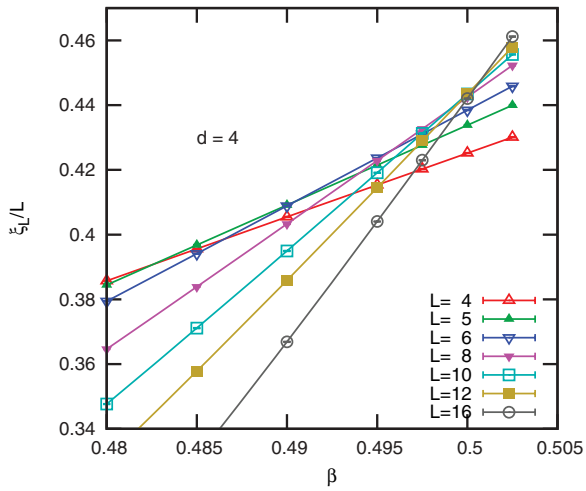

FIG. 4. (Color online) An enlarged view of the data in Fig. 3 showing the region of the intersections.

Next we compute η from the quotients of $\chi_{\rm SG}$, defined in Eq. (18), at the crossings of ξ_L/L and U_4, which are shown in Table VI and Figs. 4 and 5. Assuming $\omega = 1.04(10)$, a linear fit to Eq. (36) with $s = 2$ and the same value of y_O ($=2-\eta$) for both quantities gives, for the largest two pairs of sizes, $Q \equiv 2^{2-\eta} = 4.949(45)[^{+8}_{-14}]$, $\chi^2/\mathcal{N}_{\rm DOF} = 0.42/1$, in which the numbers in square brackets, $[\cdots]$, correspond to the errors due to the uncertainty in the value of ω. This fit is shown in Fig. 7 by the dashed lines.

On the other hand, a quadratic fit to $Q(\chi_{\rm SG}) = Q + B_1 L^{-\omega} + B_2 L^{-2\omega}$ using the largest three pairs gives $Q = 5.039(10)[^{+20}_{-16}]$, $\chi^2/\mathcal{N}_{\rm DOF} = 0.076/1$, which is also an acceptable fit, shown by the solid lines in Fig. 7.

If we assume the larger value for ω discussed above, namely, $\omega = 1.29(26)$, we find that only a quadratic fit is acceptable, and the value for Q is $Q = 4.962(30)[6]$, $\chi^2/\mathcal{N}_{\rm DOF} = 0.011/1$, which is intermediate between the two previous values of Q. We can summarize all the numbers with the

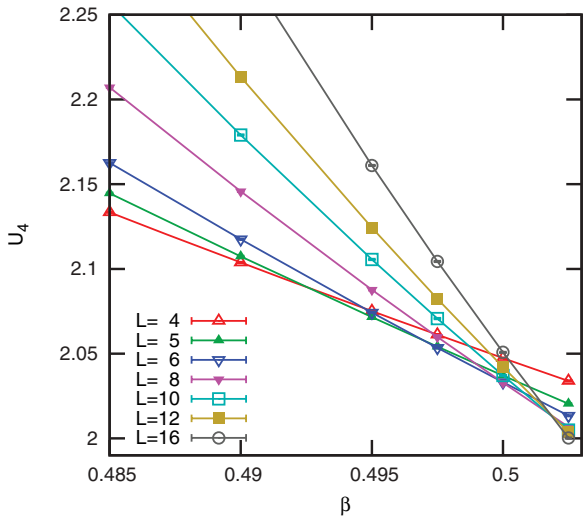

FIG. 5. (Color online) An enlarged view of the data for U_4 for the 4D model showing the region of the intersections.

TABLE IV. Inverse temperatures β_L^*, where data for sizes L and $2L$ intersect, i.e., where the quotient Q is equal to unity, for ξ_L/L and the ratio of moments U_4, for the 4D short-range model.

L	β_L^* where $Q(\xi_L/L)=1$	β_L^* where $Q(U_4)=1$
4	0.49113 ± 0.00009	0.49725 ± 0.00011
5	0.49598 ± 0.00007	0.50001 ± 0.00009
6	0.49825 ± 0.00006	0.50118 ± 0.00008
8	0.50012 ± 0.00005	0.50180 ± 0.00006

value

$$Q \equiv 2^{2-\eta} = 4.994(45). \quad (44)$$

The central value is shown as the solid horizontal line in Fig. 7, and the error bars are indicated by the dotted horizontal lines. Equation (44) gives

$$\eta_{\rm SR}(4) = -0.320(13). \quad (45)$$

To compute ν we have used the quotients for the β derivative of ξ at the crossings of ξ_L/L. The values for each pair are given in Table VII. Taking $\omega = 1.04(10)$ we obtain fitting the three largest pairs, to Eq. (36) for $s = 2$,

$$Q \equiv 2^{1+1/\nu} = 3.828(9)[8], \quad \chi^2/\mathcal{N}_{\rm DOF} = 0.68/1, \quad (46)$$

which gives $\nu = 1.068(4)[3]$. Combining the errors we get our final estimate for ν as

$$\nu_{\rm SR}(4) = 1.068(7). \quad (47)$$

The data and the fit are shown in Fig. 8

Finally we estimate β_c by fitting the crossing points for ξ_L/L and U_4 to Eq. (30), using the previously determined values $\omega = 1.04(10)$ and $\nu = 1.068(7)$. The data have already been given in Table IV and are plotted in Fig. 9. We obtain a good fit considering only the (6,12) and (8,16) pairs:

$$\beta_c = 0.50256(14)[15], \quad \chi^2/\mathcal{N}_{\rm DOF} = 0.24/1. \quad (48)$$

This fit is shown by the dashed lines in Fig. 9.

We have tried to (roughly) take into account higher-order corrections to scaling adding a quadratic term in $L^{-\omega-1/\nu}$. We obtain a good fit with the pairs (5,10), (6,12), and (8,16):

$$\beta_c = 0.50195(34)[1], \quad \chi^2/\mathcal{N}_{\rm DOF} = 0.30/1, \quad (49)$$

and this is shown by the solid lines in Fig. 9. We can therefore safely take the value

$$\beta_c = 0.5023(6) \Rightarrow T_c = 1.9908(24) \quad (d = 4) \quad (50)$$

as our final result.

We end this section by comparing our results with previous computations by other authors. Marinari and Zuliani[38] studied the 4D spin glass with binary couplings, finding $T_c = 2.03(3)$, $\nu = 1.00(10)$, and $\eta = -0.30(5)$, in good agreement with our more accurate estimates. Jörg and Katzgraber[39] studied a different version of the 4D spin glass which is expected to belong to the same universality class. They found $\nu = 1.02(2)$ and $\eta = -0.275(25)$, which are two standard deviations from our estimate. Jörg and Katzgraber also considered the leading corrections to scaling, but found an extremely large exponent, $\omega \approx 2.5$. They were aware that such a large ω is unlikely to be correct, and they attributed their result to the small lattice sizes that they could equilibrate.

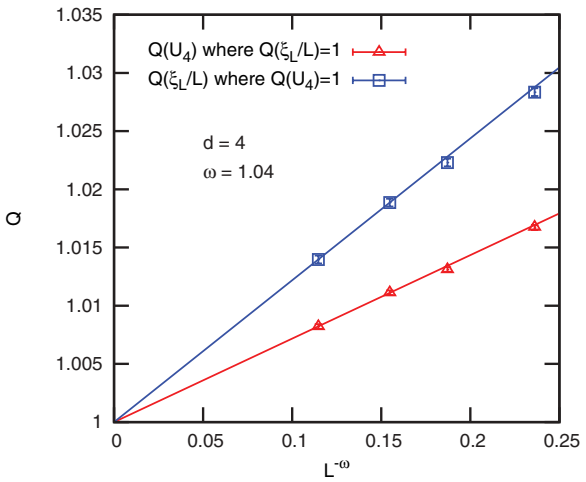

FIG. 6. (Color online) The quotient of the dimensionless quantity ξ_L/L of the 4D model at the U_4 crossing (squares) and the quotient of U_4 at the ξ_L/L crossing (triangles). The straight lines represent the best fit to Eq. (34) using the largest two sizes, with the correction-to-scaling exponent ω as an adjustable parameter.

B. One-dimensional long-range model with $\sigma = 0.790$

From Eq. (8) and the value $\eta_{\rm SR}(4) = -0.320(13)$ for the 4D model given in Eq. (45), we see that $\sigma = 0.790$ is a proxy for the 4D short-range model, at least according to the comparison of the exponents η [or equivalently of the magnetic exponents y_H; see Eq. (5)]. In this section we will see if Eq. (5) is also satisfied for the thermal exponents y_T [for which Eq. (5) can be expressed in terms of ν as shown in Eq. (9)], and the correction-to-scaling exponents ω ($=-y_u$). Since $\eta_{\rm LR}$ is known exactly, $2 - \eta_{\rm LR}(\sigma) = 2\sigma - 1$ [see Eq. (7)] we can include $\chi_{\rm SG}/L^{2\sigma-1}$ as another scale-invariant quantity to be studied.

We focus on ξ_L and $\chi_{\rm SG}/L^{2\sigma-1}$, data for which are shown in Fig. 10, and the corresponding crossing points are given in Table VIII. Our first task is to try to determine the correction-to-scaling exponent ω. We fit the quotients of ξ_L/L, U_4, and U_{22},

TABLE V. Quotients of U_4 at the crossings of ξ_L/L, and vice versa, for the 4D short-range model.

L	$Q(U_4)$ where $Q(\xi_L/L)=1$	$Q(\xi_L/L)$ where $Q(U_4)=1$
4	1.01675 ± 0.00020	1.02835 ± 0.00033
5	1.01311 ± 0.00020	1.02230 ± 0.00033
6	1.01112 ± 0.00020	1.01886 ± 0.00033
8	1.00822 ± 0.00020	1.01397 ± 0.00033

TABLE VI. Quotients of $\chi_{\rm SG}$ at the crossings of ξ_L/L and U_4 for the 4D short-range model.

L	$Q(\chi_{\rm SG})$ where $Q(\xi_L/L)=1$	$Q(\chi_{\rm SG})$ where $Q(U_4)=1$
4	4.6464 ± 0.0022	5.0077 ± 0.0045
5	4.7477 ± 0.0022	5.0368 ± 0.0046
6	4.8074 ± 0.0022	5.0547 ± 0.0047
8	4.8673 ± 0.0022	5.0522 ± 0.0047

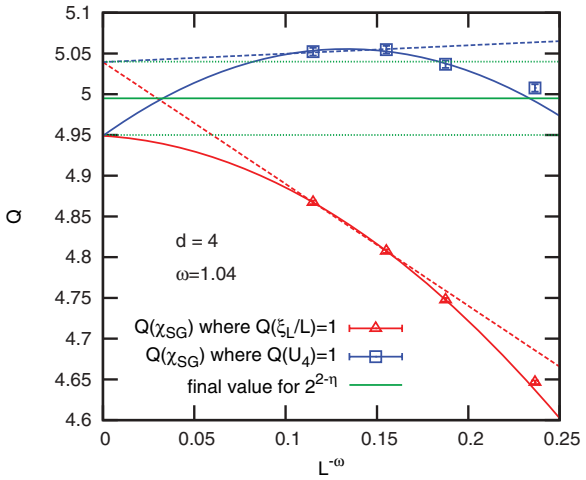

FIG. 7. (Color online) The quotients of χ_{SG} of the 4D model at the crossings of ξ_L/L (triangles) and U_4 (squares) as a function of $L^{-\omega}$, where ω has already been determined (see Fig. 6), and is given by Eq. (43). The dashed lines are the linear fit, with a common intercept on the y axis, to the two largest pairs of sizes, and the solid lines are the quadratic fit to the three largest pairs of sizes (again with a common intercept). The intercept is equal to $2^{2-\eta}$. The horizontal lines indicate the final estimate and error bars for Q given in Eq. (44). This leads to the final estimate for η in Eq. (45).

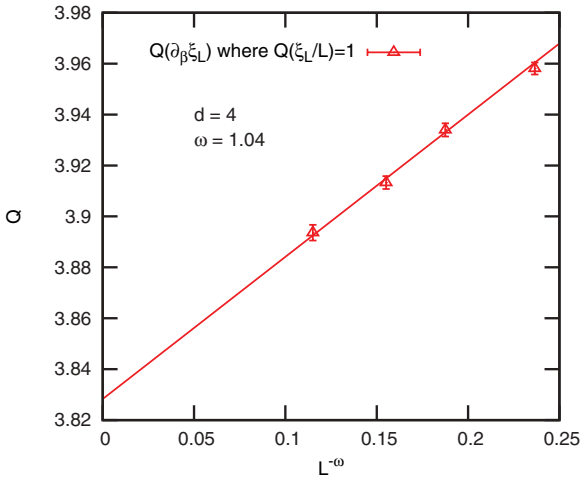

FIG. 8. (Color online) The quotient of $\partial_\beta \xi_L$ of the 4D model at the crossing of ξ_L/L. as a function of $L^{-\omega}$, where ω has already been determined (see Fig. 6), and is given by Eq. (43). The solid line is a linear fit to Eq. (36) using the three largest pairs of sizes. The intercept is equal to $2^{1+1/\nu}$. The final value of ν is given in Eq. (47).

defined in Eq. (22), at the crossing of $\chi_{SG}/L^{2\sigma-1}$, including all the $(L,2L)$ pairs. A straight-line fit, shown in Fig. 11, is acceptable:

$$\omega = 0.539(9), \quad \chi^2/\mathcal{N}_{DOF} = 16.7/14, \tag{51}$$

and has a probability of 15%. A quadratic fit to $1 + B_1 L^{-\omega} + B_2 L^{-2\omega}$ gives a better fit: $\omega = 0.29(-4+9)$, $\chi^2/\mathcal{N}_{DOF} = 7/11$. This is consistent with the value 0.26(3) expected from the correspondence in Eq. (10) and the value of ω for the 4D model given in Eq. (43). We have also tried fits in which ω is *fixed* to the value 0.26. A straight-line fit using all the data is very poor, $\chi^2/\mathcal{N}_{DOF} = 1069/15$, whereas a quadratic fit works well, $\chi^2/\mathcal{N}_{DOF} = 7.5/12$, and is shown in Fig. 12.

Altogether, we see that our data for the quotients of scale-invariant quantities do not constrain ω precisely. Any value in the range 0.25–0.55 can be considered acceptable. Fortunately, this includes the value expected from the the correspondence with the 4D model, $\omega = 0.26(3)$.

To estimate ν we consider the $(L,2L)$ quotients of the logarithmic derivatives of χ_{SG}, ξ_L, and U_4 with respect to β, at the crossings of $\chi_{SG}/L^{2\sigma-1}$. All these quotients should tend to $2^{1/\nu}$ for $L \to \infty$. A straight-line fit according to Eq. (36), allowing ω as well as the intercept Q to vary, is shown in Fig. 13. The result is

$$Q \equiv 2^{1/\nu} = 1.1703(23), \quad \chi^2/\mathcal{N}_{DOF} = 14.24/13, \tag{52}$$

$$\omega_{LR}(0.790) = 0.277(8), \tag{53}$$

which gives

$$\nu_{LR}(0.790) = 4.41(19). \tag{54}$$

This is consistent with the result 4.272(20) expected from the correspondence with the 4D model [see Eq. (9)] and

TABLE VII. Quotients of the β derivative of ξ_L at the crossings of ξ_L/L for the 4D short-range model.

L	$Q(\partial_\beta \xi_L)$ where $Q(\xi_L/L) = 1$
4	3.9581 ± 0.0024
5	3.9340 ± 0.0026
6	3.9133 ± 0.0025
8	3.8936 ± 0.0031

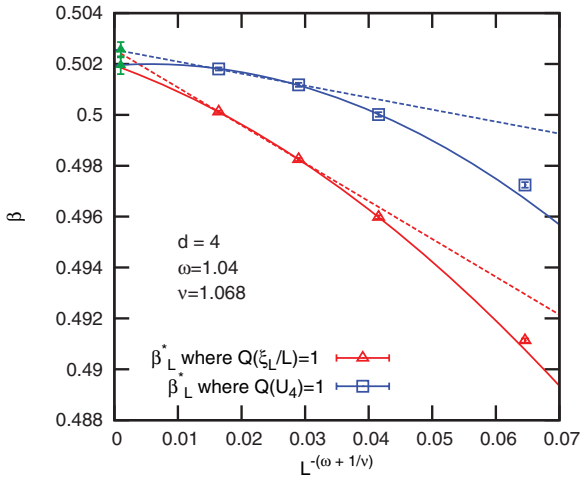

FIG. 9. (Color online) Values of β_L^*, the crossing points for ξ_L/L and U_4, for the 4D model, and fits as a function of $1/L^{\omega+1/\nu}$, for the 4D model. We used the values of ω and ν previously determined [see Eqs. (43) and (47)]. The dashed lines are the linear fit, according to Eq. (30), with a common intercept on the y axis, to the two largest pairs of sizes, and the solid lines are the quadratic fit to the three largest pairs of sizes (again with a common intercept). The intercept is the critical coupling β_c. The green data points are the estimates for β_c for the two fits, Eqs. (48) and (49).

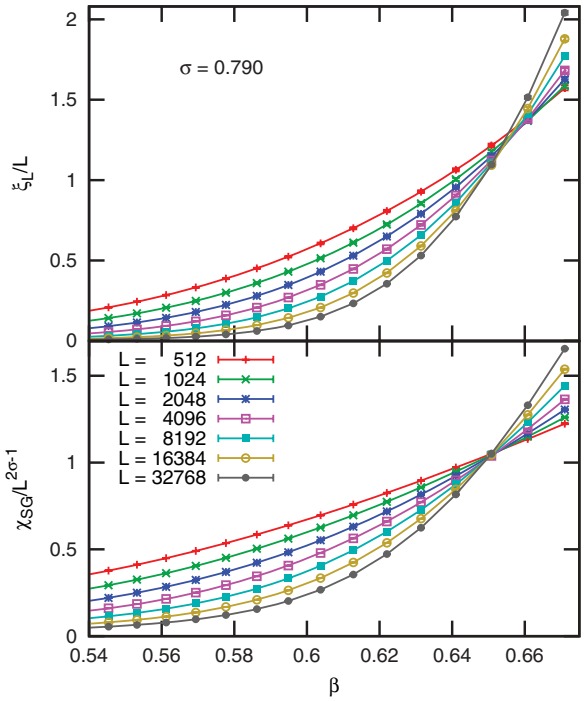

FIG. 10. (Color online) Correlation length in units of the system size (top) and scale-invariant combination of the SG susceptibility and the lattice dimension $\chi_{SG}/L^{2\sigma-1}$ (bottom), as a function of the inverse temperature β, for the LR model with $\sigma = 0.790$. For both quantities, the curves for the different L should cross at temperatures that approach the critical point when L grows; see Eq. (30).

the 4D value of ν given in Eq. (47), $\nu_{SR}(4) = 1.068(7)$. It is surprising that the fits in Fig. 13 give such a good precision for ω, better than using quotients of scale-invariant quantities which we showed in Figs. 11 and 12. The result $\omega = 0.277(8)$ is consistent with that expected from the 4D correspondence, $\omega = 0.26(3)$. We have also tried a quadratic fit, which gives $Q = 1.1742(58)[22]$, $\chi^2/\mathcal{N}_{DOF} = 9.54/11$, and a linear fit discarding the $L = 512$ data, which gives $Q = 1.1683(15)[62]$, $\chi^2/\mathcal{N}_{DOF} = 7.56/8$ [both of these fits used the value for ω obtained from the correspondence with the 4D model, $\omega = \omega_{SR}(4)/4 = 0.26(3)$]. These results are all consistent with Eq. (54) which we therefore take as our final estimate for $\nu_{LR}(0.790)$.

However, the alert reader will recall from Sec. III that the β derivative of $\chi_{SG}/L^{2\sigma-1}$ suffers from *two* types of correction to scaling, one of order $L^{-\omega}$ and the other of order

TABLE VIII. Inverse temperatures β_L^*, where data for sizes L and $2L$ intersect, i.e., where the quotient Q is equal to unity, for $\chi_{SG}/L^{2\sigma-1}$ and ξ_L/L for the LR model with $\sigma = 0.790$.

L	β_L^* where $Q(\chi_{SG}/L^{2\sigma-1})=1$	β_L^* where $Q(\xi_L/L)=1$
512	0.6538 ± 0.0020	0.6665 ± 0.0066
1024	0.6532 ± 0.0018	0.6598 ± 0.0050
2048	0.6516 ± 0.0014	0.6586 ± 0.0038
4096	0.6498 ± 0.0012	0.6545 ± 0.0031
8192	0.6500 ± 0.0009	0.6541 ± 0.0023
16384	0.6492 ± 0.0008	0.6501 ± 0.0019

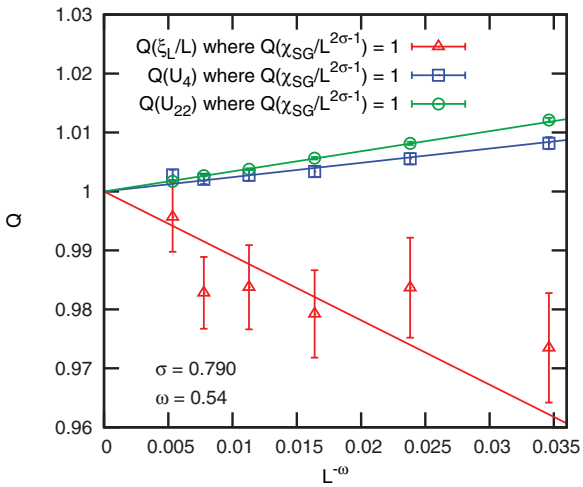

FIG. 11. (Color online) The quotients of dimensionless quantities ξ_L/L, U_4, and U_{22} for $\sigma = 0.790$ at the crossing of $\chi_{SG}/L^{2\sigma-1}$. The straight lines represent the best fit to Eq. (34) using all the data, with the correction-to-scaling exponent ω as an adjustable parameter.

$L^{-1/\nu}$; see Eqs. (41) and (42). The relationship between the LR and SR exponents in Eqs. (9) and (10), combined with our numerical results for the $d = 4$ SR model in Sec. V A, suggests that the two corrections to scaling are very similar for $\sigma = 0.790$ because $\omega_{SR}(4) \simeq 1/\nu_{SR}(4)$. This implies that the two corrections can be lumped together into a single term to a good approximation. Indeed, we have succeeded in analyzing our numerical data by considering only the scaling corrections of order $L^{-\omega}$. Therefore, although we take Eq. (53) as our final estimate for $\omega_{LR}(0.790)$, we warn that its error is probably underestimated, due to the oversimplification in the functional form for the scaling corrections.

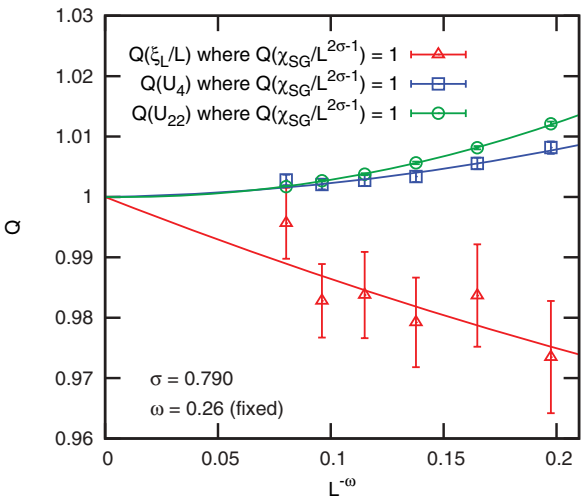

FIG. 12. (Color online) The quotients of dimensionless quantities ξ_L/L, U_4, and U_{22} at the crossings of $\chi_{SG}/L^{2\sigma-1}$ for $\sigma = 0.790$. The lines represent the best quadratic fits as functions of $1/L^{\omega}$, using all the data, where ω is fixed at 0.26 (=1.04/4), the value expected from the correspondence with the 4D model, for which the value of ω is given in Eq. (43).

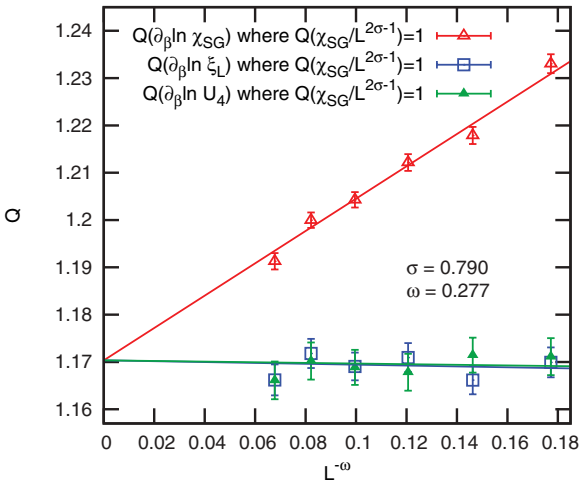

FIG. 13. (Color online) The quotients of $\partial_\beta \ln \xi_L$, $\partial_\beta \ln U_4$, and $\partial_\beta \ln \chi_{SG}$ at the crossings of $\chi_{SG}/L^{2\sigma-1}$ for $\sigma = 0.790$. The lines represent the best straight-line fits as functions of $1/L^\omega$, using all the data, in which ω, as well as the intercept $Q = 2^{1/\nu}$, are fit parameters.

By contrast, we shall see in Sec. V C that for $\sigma = 0.896$ the corrections of order $L^{-1/\nu}$ turn out to be dominant, and will need to be taken into account explicitly.

Finally, in this section, we determine β_c by fitting the crossing points of ξ_L/L and $\chi_{SG}/L^{2\sigma-1}$ shown in Table VIII to Eq. (30), assuming the values in Eqs. (53) and (54), $\omega = 0.277(8)$, $\nu = 4.41(19)$. The plot is shown in Fig. 14, and the result is $\beta_c = 0.64805(39)[2]$. Combining the errors gives

$$\beta_c = 0.64805(41) \;\Rightarrow\; T_c = 1.5431(10), \qquad (55)$$

with $\chi^2/\mathcal{N}_{DOF} = 4.47/10$. Note that the contribution to the error from the uncertainty in ω is very small.

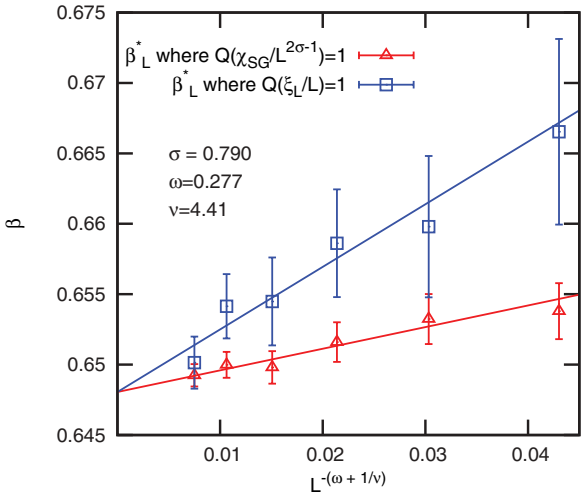

FIG. 14. (Color online) Values of β_L^*, the crossing points for ξ_L/L and $\chi_{SG}/L^{2\sigma-1}$, for $\sigma = 0.790$, as a function of $1/L^{\omega+1/\nu}$, where the values of ω and ν are fixed at the values given in Eqs. (53) and (54). The intercept is the critical coupling β_c.

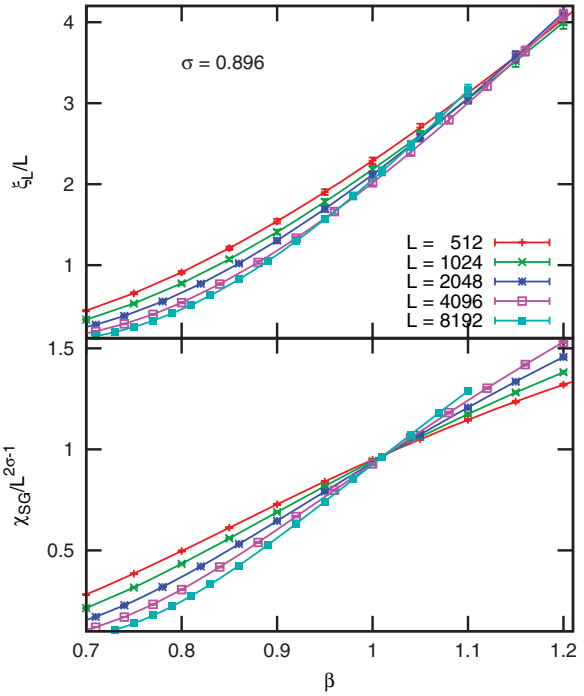

FIG. 15. (Color online) Correlation length in units of the system size (top) and scale-invariant combination of the SG susceptibility and the lattice dimension $\chi_{SG}/L^{2\sigma-1}$ (bottom), as a function of the inverse temperature β, for the LR model with $\sigma = 0.896$. For both quantities, the curves for the different L should cross at temperatures that approach the critical point when L grows; see Eq. (30).

C. One-dimensional long-range model with $\sigma = 0.896$

According to Eq. (8) and the value of η for the 3D model given in Ref. 18, $\eta_{SR}(3) = -0.375(10)$, $\sigma = 0.896$ is a proxy for 3D, at least according to the comparison of the exponents η (or equivalently of the magnetic exponents y_H). We now attempt to see if the correspondence also works for the exponents ω and ν.

As we show in Fig. 15, ξ_L/L displays a rather marginal behavior for this value of σ. We are not able to resolve the crossing temperatures for this dimensionless quantity. On the other hand, crossing points of $\chi_{SG}/L^{2\sigma-1}$ are easily identified. Our interpretation of these findings is that, for this value of σ, we are fairly close to the critical value σ_l, such that for $\sigma > \sigma_l$ there is no longer a SG phase; see Sec. I. It is expected that[14] $\sigma_l = 1$ since this corresponds to $d - 2 + \eta = 0$ with $d = 1$ and $\eta = \eta_{LR}(\sigma) = 3 - 2\sigma$. Hence a transition is expected for $\sigma = 0.896$. It is easier to find crossing points from $\chi_{SG}/L^{2\sigma-1}$, because, in the SG phase, this value scales as L^a with an exponent a larger than the corresponding one for ξ_L/L, so we feel that our results for $\sigma = 0.896$ are consistent with the expected transition.

Unfortunately, plots of dimensionless quantities do not allow us to determine ω because there is very little size dependence in the quotients. This is illustrated in Fig. 16 which shows quotients of ξ_L/L, U_4, and U_{22} at crossings of $\chi_{SG}/L^{2\sigma-1}$.

To determine ν we first consider the quotients of the logarithmic derivatives with respect to β of the dimensionless quantities ξ_L and U_4 at the $\chi_{SG}/L^{2\sigma-1}$ crossing (Fig. 17). A

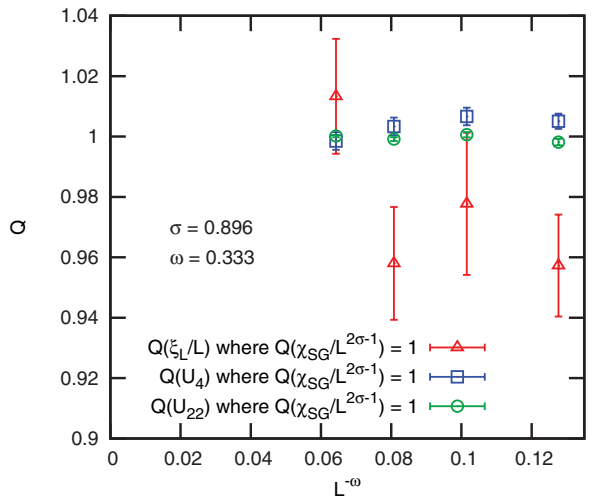

FIG. 16. (Color online) Quotients of the dimensionless quantities ξ_L/L, U_4, and U_{22} at the crossings of $\chi_{SG}/L^{2\sigma-1}$ for $\sigma = 0.896$. Compared to the error bars there is very little size dependence so the data are inadequate to determine the correction-to-scaling exponent ω.

fit to $Q + B_1 L^{-\omega}$ does not allow us to find ω, so we fix the value $\omega = 0.33(3)$, obtained from Eq. (5) and the result of Hasenbusch *et al.*[18] that $\omega_{SR}(3) = 1.0(1)$, obtaining

$$Q \equiv 2^{1/\nu} = 1.0890(202)[2], \quad \chi^2/\mathcal{N}_{DOF} = 1.14/5, \qquad (56)$$

which determines ν to be in the range $5.7 < \nu < 10.4$. Notice the smallness of the error bars coming from the ω error, or conversely the difficulty of determining ω from these quantities.

We also tried a more complex fit including the quotients of logarithmic derivatives of the scale-invariant quantity $\chi_{SG}/L^{2\sigma-1}$. As discussed in Sec. III, this derivative (but only this one) suffers from additional scaling corrections of order $L^{-1/\nu}$. Note that, according to Eqs. (9) and (10) and the SR values[18] $\omega_{SR}(3) = 1.0(1)$, $\nu_{SR}(3) = 2.45(15)$, we expect $\omega_{LR} \approx 0.33$ and $1/\nu_{LR} \approx 0.14$, so the corrections of order $L^{-1/\nu}$ are dominant. We therefore fit the data for the quotients of the logarithmic derivative of $\chi_{SG}/L^{2\sigma-1}$ to Eq. (42), while for the quotients of the logarithmic derivatives of U_4 and ξ_L/L we use Eq. (36) with $y_O = 1/\nu$, which corresponds to $B_2 = 0$. The data is shown in Fig. 17.

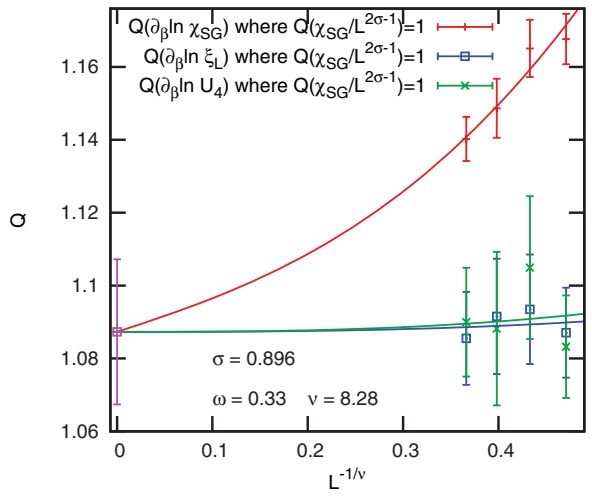

FIG. 17. (Color online) The quotients of $\partial_\beta \ln \xi_L$, $\partial_\beta \ln U_4$, and $\partial_\beta \ln \chi_{SG}$ at the crossings of $\chi_{SG}/L^{2\sigma-1}$ for $\sigma = 0.896$. For $\partial_\beta \ln \xi_L$ and $\partial_\beta \ln U_4$ the lines are fits to functions of type $Q + B_1 L^{-\omega}$, where $Q = 2^{1/\nu}$; see Eq. (36). For χ_{SG} we need to consider also an $L^{-1/\nu}$ term; see Eq. (42). The ω value is fixed to the value 0.33 expected from the 3D data of Hasenbusch *et al.* (Ref. 18) who find $\omega_{SR}(3) = 1.0(1)$, and Eq. (10), while the value of ν is a fit parameter.

To obtain a reliable fit, we need to fix the value of ω and, as above, we take this to be $\omega = 0.33(3)$, obtaining

$$Q \equiv 2^{1/\nu} = 1.087(199)[3], \quad \chi^2/\mathcal{N}_{DOF} = 1.54/7, \qquad (57)$$

which determines ν to be in the range $6.8 < \nu < 10.6$, so our estimate for ν is

$$\nu_{LR}(0.896) = 8.7(1.9). \qquad (58)$$

Again, the effect of the ω uncertainty is very small. We have tried to bound the ω value from this fit, but the result is almost useless [$\omega \in (0,0.97)$].

Finally we discuss the value of β_c. We do not see any evolution of β_c with L. However, we perform several fits to estimate the extrapolation errors. First we try a fit of the $\chi_{SG}/L^{2\sigma-1}$ crossings taking ω and ν from the 3D-derived values: $\omega = 0.33(3)$, $\nu = 7.35(45)$ so $\omega + 1/\nu = 0.47(4)$. The result is $\beta_c = 1.004(15)[1]$, with $\chi^2/\mathcal{N}_{DOF} = 0.24/2$. If we use $\omega = 0.33(3)$ but the ν value obtained above, $\nu = 8.7(1.9)$, i.e., $\omega + 1/\nu = 0.44(5)$, we get $\beta_c = 1.003(16)[2]$, $\chi^2/\mathcal{N}_{DOF} = 0.23/2$.

These last two results are statistically correlated, and we take the latter as our final estimate:

$$\beta_c = 1.003(18) \Rightarrow T_c = 0.997(18). \qquad (59)$$

VI. CONCLUSIONS

The purpose of this paper is to see if there is a value of σ for the long-range spin-glass model which corresponds precisely to a short-range four-dimensional spin glass, and (with a different value of σ) to a three-dimensional spin glass, in the sense that *all* the LR and SR exponents, in particular, η, ν, and ω, match in the sense of Eqs. (5)–(10). Since η_{LR} is given exactly by the simple expression in Eq. (7), we have chosen two values of σ, 0.790 and 0.896, as proxies for 4D and 3D, respectively, since the values of η match according to Eq. (8). The question, then, is whether the *other* exponents, ω and ν, match according to Eqs. (10) and (9).

Our results for ω and ν are summarized in Table IX. For the case of 4D, the correspondence works well, the values for the exponents being consistent with Eqs. (9) and (10) within reasonably modest error bars. However, for 3D, we are not able to establish a sharp connection, since, for the corresponding long-range model, $\sigma = 0.896$, we cannot determine ω. If we *assume* that the value of $\omega_{LR}(0.896)$ is that given by the matching formula, Eq. (10), with the value of ω from the 3D simulations,[18] namely, $\omega_{LR}(0.896) = 0.33(3)$, then we find $\nu_{LR} = 8.7 \pm 1.9$ which *is* consistent with $3\nu_{SR}(3) = 7.35 \pm 0.45$.

TABLE IX. Summary of results for critical exponents of the short-range models in 3D and 4D, the expected (proxy) results for the long-range models based on the short-range results and the connection in Eq. (5), and the actual results for the long-range models. It was not possible to estimate ω for the long-range model with $\sigma = 0.896$. If we assume that it is given by the matching formula, ω_{SR}/d, then we obtain the result for $\nu_{LR}(0.896)$ shown in the table. The 3D results are from Ref. 18, and all other results are from the present work.

	$d = 4$, $\sigma = 0.790$	$d = 3$, $\sigma = 0.896$
$\omega_{SR}(d)$	1.04(10)	1.0(1)
$\omega_{SR}(d)/d$	0.26(4)	0.33(3)
$\omega_{LR}(\sigma)$	0.277(8)	–
$\nu_{SR}(d)$	1.068(5)	2.45(15)
$d\,\nu_{SR}(d)$	4.272(20)	7.35(45)
$\nu_{LR}(\sigma)$	4.41(19)	8.7(1.9)

While it seems unlikely to us that all the critical exponents of the LR and SR models match exactly according to Eq. (5), our results indicate that these equations are satisfied to a good approximation, and hence the critical behaviors of the SR and corresponding LR models are very similar. Whether this similarity extends to the more subtle question of the nature of the spin-glass phase below T_c remains to be seen.

ACKNOWLEDGMENTS

We thank G. Parisi and M. Moore for discussions. A.P.Y. acknowledges support from the NSF through Grant No. DMR-0906366 and a generous allocation of computer time from the Hierarchical Systems Research Foundation. The short-range simulations, and part of the long-range simulations, were carried out on ARAGRID and BIFI computers. R.A.B., L.A.F., and V.M.M. acknowledge partial financial support from MICINN, Spain, Contract No. FIS2009-12648-C03. R.A.B. was also supported by the FPI Program (Diputación de Aragón, Spain). V.M.M. acknowledges the hospitality of the Physics Department of UCSC (visit funded by the Del Amo Foundation), where part of this work was performed.

[1] K. Binder and A. P. Young, Rev. Mod. Phys. **58**, 801 (1986).
[2] *Finite Size Scaling and Numerical Simulation of Statistical Systems*, edited by V. Privman (World Scientific, Singapore, 1990).
[3] D. Amit and V. Matin-Mayor, *Field Theory, the Renormalization Group and Critical Phenomena* (World Scientific, Singapore, 2005).
[4] H. G. Katzgraber and A. P. Young, Phys. Rev. B **67**, 134410 (2003).
[5] H. G. Katzgraber and A. P. Young, Phys. Rev. B **68**, 224408 (2003).
[6] H. G. Katzgraber and A. P. Young, Phys. Rev. B **72**, 184416 (2005).
[7] H. G. Katzgraber, D. Larson, and A. P. Young, Phys. Rev. Lett. **102**, 177205 (2009).
[8] D. Larson, H. G. Katzgraber, M. A. Moore, and A. P. Young, Phys. Rev. B **81**, 064415 (2010).
[9] A. Sharma and A. P. Young, Phys. Rev. B **83**, 214405 (2011).
[10] L. Leuzzi, G. Parisi, F. Ricci-Tersenghi, and J. J. Ruiz-Lorenzo, Phys. Rev. Lett. **101**, 107203 (2008).
[11] L. Leuzzi, G. Parisi, F. Ricci-Tersenghi, and J. J. Ruiz-Lorenzo, Phys. Rev. Lett. **103**, 267201 (2009).
[12] L. Leuzzi, G. Parisi, F. Ricci-Tersenghi, and J. J. Ruiz-Lorenzo, Philos. Mag. **91**, 1917 (2011).
[13] A. B. Harris, T. C. Lubensky, and J.-H. Chen, Phys. Rev. Lett. **36**, 415 (1976).
[14] G. Kotliar, P. W. Anderson, and D. L. Stein, Phys. Rev. B **27**, 602 (1983).
[15] M. A. Moore (private communication).
[16] G. Parisi (private communication).
[17] M. E. Fisher, S.-k. Ma, and B. G. Nickel, Phys. Rev. Lett. **29**, 917 (1972).
[18] M. Hasenbusch, A. Pelissetto, and E. Vicari, Phys. Rev. B **78**, 214205 (2008).
[19] M. E. J. Newman and G. T. Barkema, *Monte Carlo Methods in Statistical Physics* (Oxford University Press, New York, 1999).
[20] Actually, some long-range models with power-law interactions can be simulated efficiently. Unfortunately, the cluster algorithms of Refs. 21 and 22 do not work for spin glasses. On the other hand, the stochastic cutoff method (Ref. 23) does not rely on a cluster update, but its efficiency for simulating spin glasses with long-range interactions is yet to be assessed.
[21] E. Luijten and H. W. J. Blöte, Phys. Rev. Lett. **76**, 1557 (1996).
[22] K. Fukui and S. Todo, J. Comput. Phys. **228**, 2629 (2009).
[23] M. Sasaki and F. Matsubara, J. Phys. Soc. Jpn. **77**, 024004 (2008).
[24] F. Beyer, M. Weigel, and M. A. Moore, Phys. Rev. B **86**, 014431 (2012).
[25] M. Wittmann and A. P. Young, Phys. Rev. E **85**, 041104 (2012).
[26] L. Viana and A. J. Bray, J. Phys. C **18**, 3037 (1985).
[27] L. A. Fernández, V. Martín-Mayor, G. Parisi, and B. Seoane, Phys. Rev. B **81**, 134403 (2010).
[28] We run the Monte Carlo of the bonds for 10^6 sweeps. We are confident about graph equilibration because we compared the outcomes of widely differing starting points for the simulation: either a graph with the topology of a crystal with periodic boundary conditions, or the random graph described in the main text. For either type of starting point, we compared several graph properties, in particular the bond-length distribution and the "Hamiltonian" defined in Eq. (15). In all cases studied, we found that memory of the starting configuration was lost after 10^5 sweeps, but we simulated for a total 10^6 sweeps to be on the safe side.
[29] B. Cooper, B. Freedman, and D. Preston, Nucl. Phys. B **210**, 210 (1982).
[30] M. Palassini and S. Caracciolo, Phys. Rev. Lett. **82**, 5128 (1999).
[31] H. G. Ballesteros, A. Cruz, L. A. Fernandez, V. Martin-Mayor, J. Pech, J. J. Ruiz-Lorenzo, A. Tarancon, P. Tellez, C. L. Ullod, and C. Ungil, Phys. Rev. B **62**, 14237 (2000).
[32] K. Binder, Z. Phys. B **43**, 119 (1981).

[33]H. G. Ballesteros, L. A. Fernandez, V. Martin-Mayor, J. Pech, and A. Muñoz Sudupe, Phys. Lett. B **387**, 125 (1996).
[34]M. P. Nightingale, Physica A **83**, 561 (1976).
[35]H. G. Ballesteros, L. A. Fernández, V. Martin-Mayor, A. Muñoz Sudupe, G. Parisi, and J. J. Ruiz-Lorenzo, Phys. Rev. B **58**, 2740 (1998).
[36]M. Weigel and W. Janke, Phys. Rev. Lett. **102**, 100601 (2009).
[37]K. Hukushima and K. Nemoto, J. Phys. Soc. Jpn. **65**, 1604 (1996).
[38]E. Marinari and F. Zuliani, J. Phys. A **32**, 7447 (1999).
[39]T. Jörg and H. G. Katzgraber, Phys. Rev. B **77**, 214426 (2008).